

ORIGINAL ARTICLE

Tunable 3D printed multi-material composites to enhance tissue fidelity for surgical simulation

Justine Garcia,^a Mansour AlOmrani,^b Alexander Emmott,^c Rosaire Mongrain,^a Kevin Lachapelle^b and Richard L. Leask^{c,*}

^aMechanical Engineering, McGill University, Montreal, Quebec, Canada; ^bCardiac Surgery, McGill University Health Network, Montreal, Quebec, Canada; ^cChemical Engineering, McGill University, Montreal, Quebec, Canada

*Corresponding author at: Chemical Engineering, McGill University, Wong Building, 3610 University Street, Montreal, Quebec H3A 0C5, Canada. Email: richard.leask@mcgill.ca

Date accepted for publication: 22 November 2018

Abstract

Background and aim: Medical simulation is an important component in surgical education. Unfortunately, there are very few 3D printed materials that have the tissue fidelity needed for enhanced learning of cardiovascular surgical techniques. Therefore, we sought to determine if we could develop 3D printed composites to better reflect the tissue mechanical properties of the ascending aorta. **Materials and method:** 3D printed composites were created using commercially available materials for a Connex3 Objet500 3D printer (Stratasys, Eden Prairie, USA). Support material (SUP705) as well as rigid zigzag Vero fibres were systematically combined with an elastic polymer (TGPF930). The mechanical properties were evaluated in equi-biaxial tensile (tensile stiffness and viscoelasticity), nano-indentation (compressive stiffness) and suture retention strength (strength) (SRS) tests for comparisons with normal ascending aortas (AA) and ascending aortas with aneurysm (AA aneurysm). **Results:** Compared with TGPF930 (unpaired t test), the insertion of support material reduced the SRS (TGPF930: 4.45 ± 0.49 N, $n = 3$; TGPF930 + SUP705: 2.57 ± 0.32 N, $n = 3$; $P = 0.0023$) and compressive modulus (TGPF930: 0.61 ± 0.08 MPa, $n = 6$; TGPF930 + SUP705: 0.38 ± 0.06 MPa, $n = 6$; $P = 0.0002$). Embedding Vero fibres increased the SRS (TGPF930: 4.45 ± 0.49 N, $n = 3$; TGPF930 + Vero: 5.39 ± 0.65 N, $n = 3$; $P = 0.0037$), compressive modulus (TGPF930: 0.61 ± 0.08 MPa, $n = 6$; TGPF930 + Vero: 0.85 ± 0.07 MPa, $n = 6$; $P = 0.0003$) and allowed for tuning the mechanical directional dependency of the composite. When all three components were combined, similarities were found with aortic tissue in terms of SRS (three-material composite: 4.25 ± 0.67 N, $n = 3$; AA aneurysm: 5.31 ± 2.71 N, $n = 3$; $P = 0.6177$) and compressive modulus (three-material composite: 0.39 ± 0.03 MPa, $n = 6$; AA aneurysm: 0.36 ± 0.12 MPa, $n = 4$; $P = 0.4485$). **Conclusion:** The study has shown that the insertions of fibres and/or support material in a TGPF930 structure can control the mechanical properties of the 3D printed composites. We were able to simulate ex vivo passive tissue characteristics of aortas, therefore improving on the current homogeneous 3D printed TGPF930 material often used in surgical education.

Keywords: surgical simulation; 3D printing; simulation; ascending aortic tissue; biomechanics; 3D printed composite

Introduction

Simulation is an important tool in medical education because it has been shown to enhance the learning and acquisition of basic technical skills outside the operating room.¹ Surgical simulators are often made with synthetic material (e.g. latex, silicone), which acts as a surrogate for human tissue. Such surgical simulators lack the anatomic, tissue and physiologic fidelity required for advanced surgical training. Biological tissues, such as animal and cadaveric material, provide excellent tissue fidelity, however they are expensive, lack patient-specific pathologies and have limited physiologic realism. For these

reasons, we sought to determine if we could develop a 3D printing strategy to better reflect the anatomic, physiologic and tissue fidelity needed for surgical simulation.

Ascending aortas (AA) are frequently involved in cardiothoracic procedures where they are manipulated, cannulated, cut, sewed and resected or reconstructed by surgeons. The vessel is very elastic and naturally designed to absorb the energy of systole and redistribute it through viscoelastic recoil during diastole (Windkessel effect). Pathologies of the AA greatly change the mechanical properties and function of the AA. With disease, the AA stiffens,

increases energy loss and loses its mechanical directional dependency.^{2,3} The energy loss is the amount of energy absorbed by the vessels during cyclic loading and is therefore a measure of the viscoelasticity of the tissue, which estimates the ability of the material to perform a Windkessel function. Therefore, controlling the material properties of synthetic aortic tissues for realistic training models is important because it would provide trainees with the haptics of a large panel of potential pathologies.

This study aims to describe our process and technique for creating 3D printed material composites with variable and controllable mechanical properties to simulate aortic walls. Given the heterogenous nature of the AA and its tendency to change its mechanical characteristics in diseased states, we elected to approach the problem of tissue fidelity by using a fibrous multi-material composite from commercially available products. The material construct properties were compared and validated with ex vivo passive normal and abnormal freshly harvested aortic tissue.

Materials and methods

Creation of the heterogeneous synthetic aortic tissue

To guide the development of our synthetic tissues, we first evaluated a flexible 3D printable material Tangoplus FullCure 930 (TGPF930) to which brittle support material (SUP705) and rigid Verowhite (Vero) were added to change the properties of the structure. All resins were available for use with a Connex3 Objet500 (Stratasys, Eden Prairie, USA). Pure TGPF930 has previously been used to 3D print synthetic arteries,^{4,5} mitral valves⁶ and cerebral aneurysms.⁷ It is relatively elastic, homogeneous and isotropic when printed by Polyjet technology, so limited in its ability to recreate different tissue pathologies. We used TGPF930 as a base material to create two- and three-material composites to tune the mechanical properties of our synthetic aortic tissue. The steps can be described as follows (Fig. 1):

- To soften a TGPF930 structure, we inserted brittle support material (SUP705);
- To strengthen a TGPF930 structure, we embedded two layers of rigid Vero fibres;
- To control the mechanical directional dependency, we embedded one layer of large fibres;
- To create a tunable, soft but strong composite from a TGPF930 structure, we embedded two layers of rigid Vero fibres and inserted brittle support material (SUP705).

Preliminary studies demonstrated that the size, volume density (e.g. distance between the fibres, number of layers of

fibres) and shape of the fibres (pattern, amplitude and phase) have a significant impact on the stiffness of the composite material.⁸ We therefore chose a series of candidate composites based on these preliminary studies to demonstrate how the tissue fidelity can be tuned to create synthetic AA tissue.

Mechanical evaluations of the materials

Each 3D printed sample was tested within 48 h of fabrication. Similarly, all samples were printed with the same printer and tested by the same operator, under the same conditions and with fully defined standard operating procedures. The number of 3D printed samples was limited and the distribution is assumed to be normal. Moreover, all samples were printed with the same batch of raw materials.

All aortic tissue was collected from transplant donors and patients undergoing surgery at the Royal Victoria Hospital (Montreal, Quebec, Canada) in accordance with the tri-council Ethical Conduct for Research Involving Humans. Three mechanical tests were carried out to assess the ability to tune the mechanical behaviour of the 3D printed composites (tests and outcomes in Table 1). The results are compared with normal and aneurysmal ex vivo passive tissue characteristics of human AA samples. Planar equibiaxial tensile testing was used to reveal material abilities to deform and stretch.⁹ In addition, nano-indentation testing (ASTM E2546) (also known as a compression test) was used to evaluate the stiffness in compression, thus the compressive modulus important for the haptics on a macro level and tactile properties of the material. Finally, suture retention strength (SRS) assessed the material's ability to be sewed for suturing practice.

Apparent elastic modulus and energy loss of the material: equi-biaxial tensile testing

Equi-biaxial tensile testing was carried out within 24 h of the excision. Samples of human tissue or composite material ($15 \times 15 \text{ mm}^2$) were subjected to equi-biaxial stretching at a constant strain rate (0.1 mm/s) (ELF 3200, Bose Co., Framingham, USA) in a bath at 37°C. The engineering stress and strain of the loading curves were fit to a second-order Mooney-Rivlin model.¹⁰ This model was used to calculate the apparent elastic modulus in MPa (commonly called stiffness in tensile testing, calculated with the slope of the loading curve) at 25% strain (Fig. 2a). The percentage of energy lost over the testing cycle was computed with the raw data to quantify the viscoelastic nature of the AA and 3D printed composites. The loading and unloading stress-strain curves of the aortic tissue formed a hysteresis loop as a result of a storage and release of energy¹¹ (Fig. 2a).

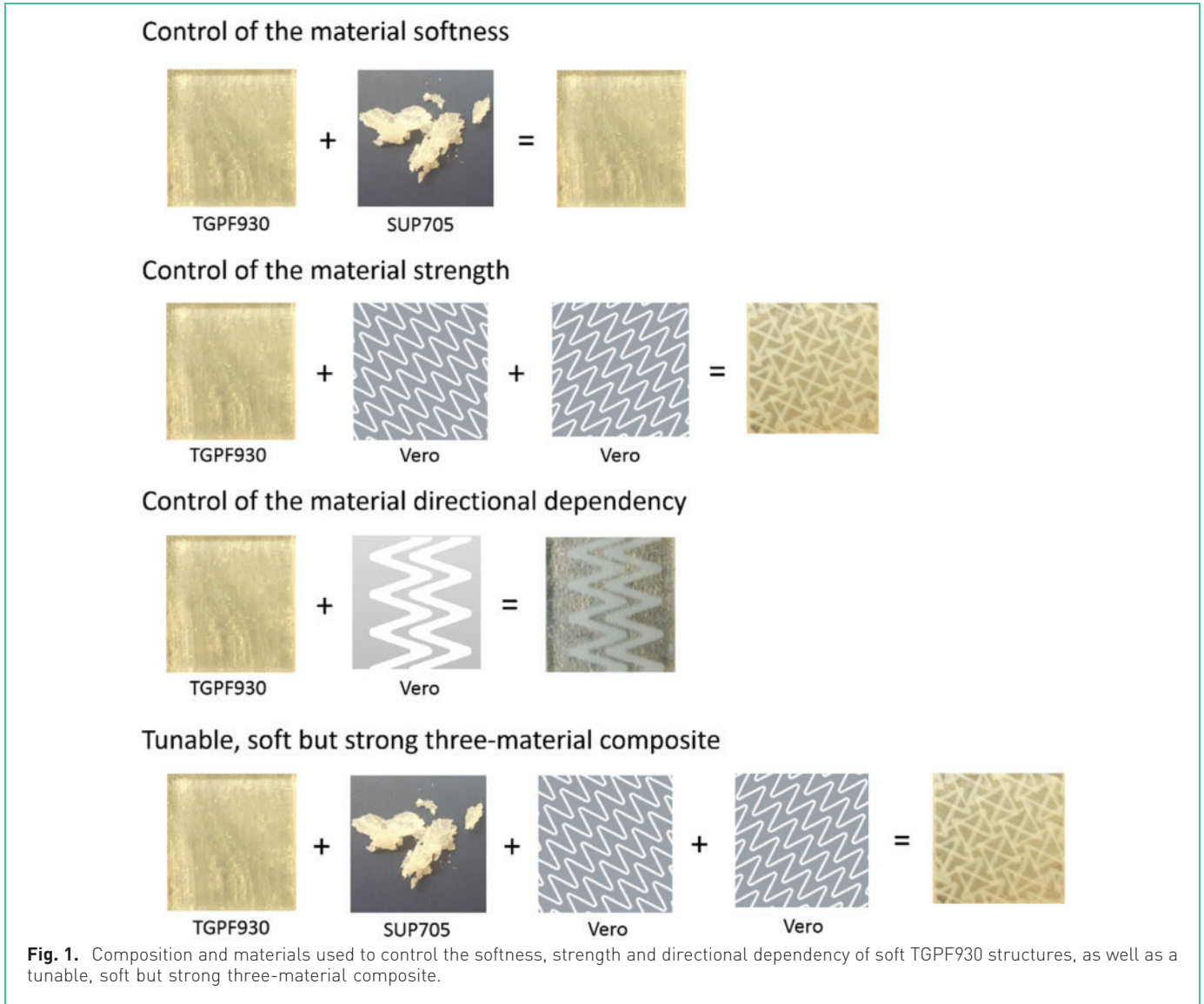


Fig. 1. Composition and materials used to control the softness, strength and directional dependency of soft TGPF930 structures, as well as a tunable, soft but strong three-material composite.

Compressive modulus: nano-indentation testing (ASTM E2546)

Compressive tests were performed with the Nanovea M1 nano-indenter (Nanovea, Irvine, USA) as per ASTM E2546 (Standard Practice for Instrumented Indentation Testing) with a 1-mm diameter spherical tip to assess the compressive stiffness of the material with a compressive modulus (E_{comp} in GPa). E_{comp} defined in the Oliver-Pharr method¹² helps to determine the tactile properties of the materials, thus their abilities to be squished. The parameter is calculated from the Poisson ratio of the material (ν is assumed to be 0.5), the apparent elastic modulus and Poisson ratio of the indenter ($E_{\text{ind}} = 200$ GPa, $\nu_{\text{ind}} = 0.1$), as well as the reduced modulus E_r (in GPa).

$$E_{\text{comp}} = \frac{(1 - \nu^2)E_{\text{ind}}E_r}{E_{\text{ind}} - E_r(1 - \nu_{\text{ind}}^2)} \quad (1)$$

Table 1. Mechanical tests and outcomes obtained from the study

| Test | Outcome |
|--------------------------------|--|
| Equi-biaxial tensile test | Apparent elastic modulus (tensile stiffness: stiff/ soft) and energy loss (viscoelasticity: inefficient/efficient Windkessel function) |
| Nano-indentation test | Compressive modulus (compressive stiffness: stiff/soft) |
| Suture retention strength test | Forces to tear the material (strength: tough/ fragile) |

E_r is derived from the material stiffness obtained from compression (S_i in mN/ μm) and projected contact area (A_c in μm^2) of the spherical tip. A_c is expressed with the radius of the sphere (R in μm), the contact depth (h_c in μm) computed with the maximum depth penetration (h_{max} in μm),

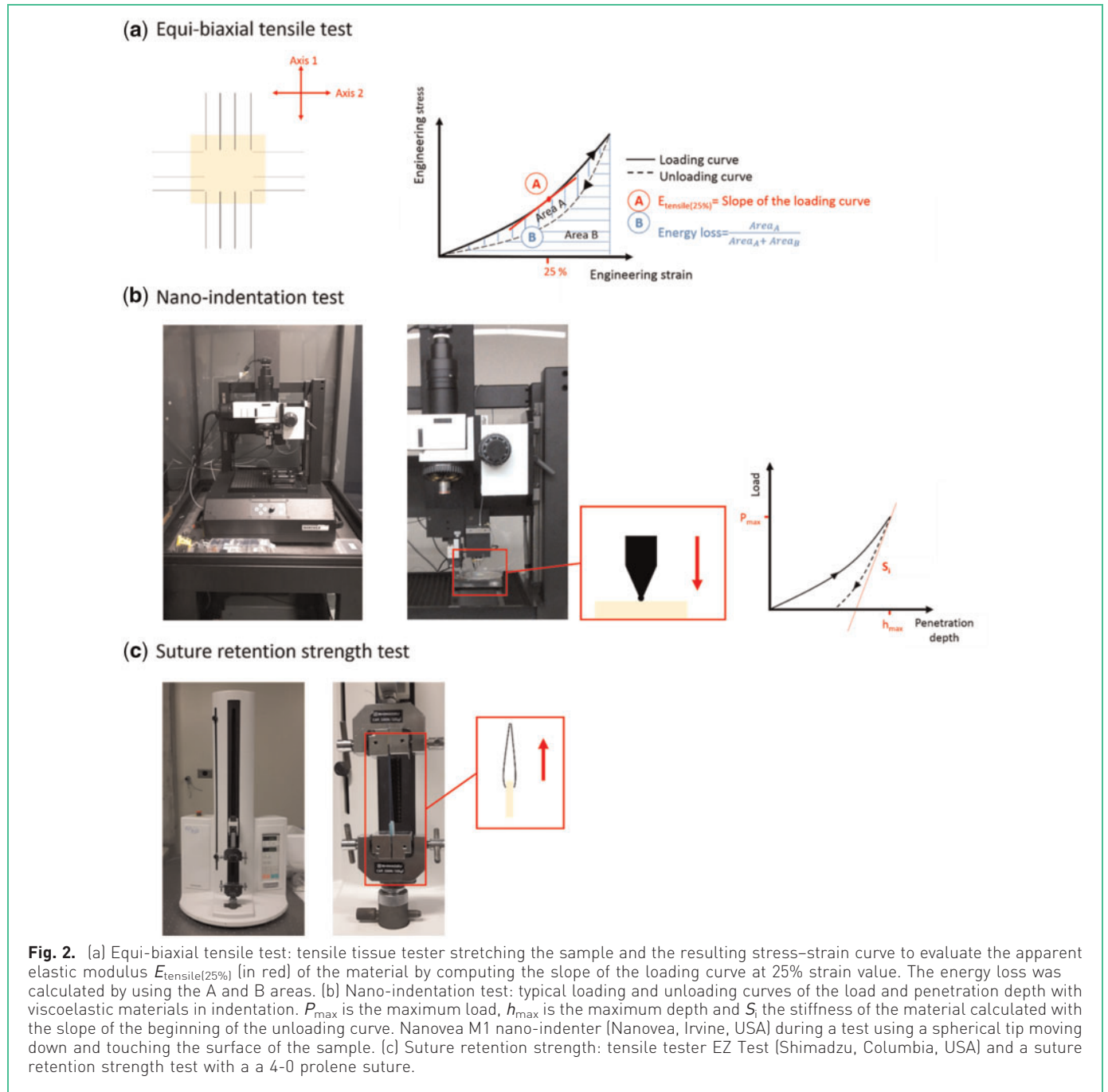


Fig. 2. (a) Equi-biaxial tensile test: tensile tissue tester stretching the sample and the resulting stress–strain curve to evaluate the apparent elastic modulus $E_{\text{tensile}(25\%)}$ (in red) of the material by computing the slope of the loading curve at 25% strain value. The energy loss was calculated by using the A and B areas. (b) Nano-indentation test: typical loading and unloading curves of the load and penetration depth with viscoelastic materials in indentation. P_{max} is the maximum load, h_{max} is the maximum depth and S_i the stiffness of the material calculated with the slope of the beginning of the unloading curve. Nanovea M1 nano-indenter (Nanovea, Irvine, USA) during a test using a spherical tip moving down and touching the surface of the sample. (c) Suture retention strength: tensile tester EZ Test (Shimadzu, Columbia, USA) and a suture retention strength test with a 4-0 prolene suture.

the maximum load (P_{max} in mN) and stiffness corresponding to the slope of the beginning of the unloading curve (Fig. 2b).

$$E_r = \frac{\sqrt{\pi} S_i}{2\sqrt{A_c}} \quad (2)$$

$$S_i = \frac{dP}{dh} \quad (3)$$

$$A_c = 2\pi R h_c \quad (4)$$

$$h_c = h_{\text{max}} - \frac{3P_{\text{max}}}{4S_i} \quad (5)$$

Suture retention strength testing

SRS is defined as the maximum force in Newtons required to tear the suture from the material. The evaluations were

performed with a 500-N vertical tensile tester EZ Test (Shimadzu, Columbia, USA) at room temperature with a single 4-0 prolene suture. The samples were pulled at 20 mm/min (Fig. 2c). Triplicates of each synthetic aorta material were tested and compared with AA tissue samples.

Statistical analyses

Data are presented as means ± standard deviation and the analyses were performed using GraphPad Prism 5 (GraphPad Software, Inc., La Jolla, USA). Comparisons between groups were done with paired and unpaired t tests. A P value of 0.05 was taken as significant. The results are summarized in Table 2.

Results

Evaluation of the aortic tissue

AAs were collected at the time of surgery. Pathologic specimens were obtained from patients with an AA aneurysm. Normal specimens were obtained from donor hearts harvested for transplants. The apparent elastic modulus (computed at 25% strain) for normal aortas ranging from 0.05 MPa to 0.09 MPa (0.08 ± 0.01 MPa and 0.06 ± 0.01 MPa for the circumferential and axial directions, n = 4 respectively). The normal energy loss of 20% to 29% (26 ± 3% and 23 ± 3% for the circumferential and axial directions,

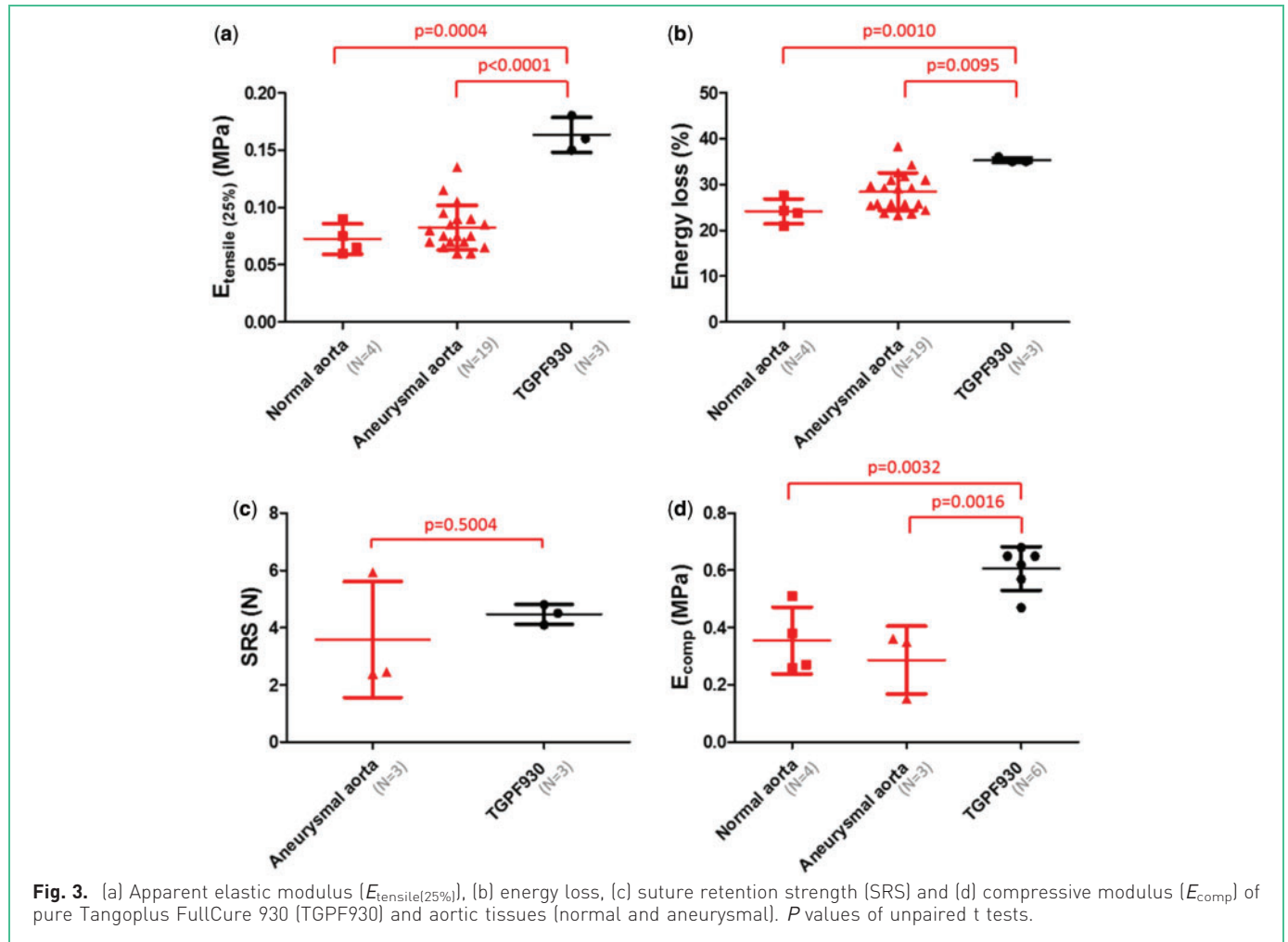
respectively). The compressive modulus of the normal donors ranged from 0.26 MPa to 0.51 MPa (0.36 ± 0.12 MPa, n = 4). Aneurysmal aortas had an apparent elastic modulus that ranged from 0.05 MPa to 0.11 MPa (0.09 ± 0.02 MPa and 0.07 ± 0.02 MPa for the circumferential and axial directions, n = 19, respectively) and an energy loss from 23% to 36% (31 ± 5% and 28 ± 5% for the circumferential and axial directions, respectively). The aneurysmal tissue compressive modulus ranged between 0.15 MPa and 0.36 MPa (0.29 ± 0.12 MPa, n = 3). Finally, the forces required to tear sutures from the aneurysmal AA were between 3.09 N and 8.33 N in the circumferential direction (5.31 ± 2.71 N, n = 3), as well as 2.38 N and 5.93 N in the axial direction (3.59 ± 2.03 N, n = 3).

Evaluation of the soft 3D printed material

We evaluated TPF930 by itself and compared the material with AA (unpaired t tests) (Fig. 3). TGPF930 had a similar SRS to the aneurysmal tissue (4.45 ± 0.49 N, n = 3, P = 0.5004). However, the printing material was stiffer and more viscous than AA (P < 0.05) due to its higher apparent elastic modulus (0.17 ± 0.02 MPa, n = 3), compressive modulus (0.61 ± 0.08 MPa, n = 6) and energy loss (39 ± 6%, n = 3). Consequently, TGPF930 is stiffer and harder than human aortic tissues.

Table 2. Test applied and outcomes for each material tested

| Material tested | Test applied | Outcome |
|--|---------------------------|--|
| TGPF930 | Equi-biaxial tensile test | Stiffer (in tensile testing) and more viscous than AA Strength similar to AA |
| | Suture retention strength | |
| | Nano-indentation test | |
| Composite: TGPF930 + SUP705 | Nano-indentation test | Softer and less resistance to suture tear than aortic tissue |
| | Suture retention strength | |
| Composite: TGPF930 + fibres (two layers) | Equi-biaxial tensile test | Stiffer (in compression and tension) and better suture tear resistance than TGPF930 |
| | Suture retention strength | |
| | Nano-indentation test | |
| Composite: TGPF930 + one layer of thick fibres | Equi-biaxial tensile test | Control of mechanical directional dependency |
| Three-material composite | Equi-biaxial tensile test | Less stiff (in tensile testing) and more viscous than composite TGPF930 + fibres (two layers) Stiffer (in tensile testing) and more viscous than aortic tissues |
| | Suture retention strength | |
| | Nano-indentation test | Similar compressive stiffness and suture strength to AA |



Control of the 3D printed material softness

The insertion of support material (SUP705) in the soft TGPF930 structure significantly softened the composite but made it too brittle. It was impossible to test the equibiaxial tensile properties of these two-material composites because every sample ripped during the experiments. In addition, it significantly decreased the SRS by 42% (TGPF930 + SUP705: 2.57 ± 0.32 N, $n = 3$, $P = 0.0023$) and the compressive modulus by 38% (TGPF930 + SUP705: 0.38 ± 0.06 MPa, $n = 6$, $P = 0.0002$) compared with pure TGPF930 (Fig. 4). Therefore, adding the brittle component (SUP705) alone to the rubber material changed the overall mechanical response of the structure but made the samples too brittle to be used as synthetic aortic tissue.

Control of the 3D printed material strength

Two layers of rigid Vero fibres were embedded in a TGPF930 structure to reproduce the extracellular matrix structure of the arteries and strengthen the material. Compared with pure TGPF930 (unpaired t test), the fibres increased the energy loss ($43 \pm 1\%$, $n = 3$, $P < 0.0001$),

SRS (difference of 21%) (5.39 ± 0.65 N, $n = 3$, $P = 0.0037$) and compressive modulus (difference of 39%) (0.85 ± 0.07 MPa, $n = 6$, $P = 0.0003$) (Fig. 5). Embedding layers of rigid Vero fibres in flexible TGPF930 structure has a significant effect on the energy loss, SRS and compressive modulus.

Control of the mechanical directional dependency of the 3D printed material

To understand if fibre embedding could control the directional dependency of the material, one layer of two thick embedded Vero fibres (cross-sectional area of 0.6×0.8 mm²) was placed in the middle of a soft TGPF930 structure. The apparent elastic modulus in tensile of the axis at which the fibres were orientated was significantly higher (16%) than the other one (0.16 ± 0.04 MPa versus 0.13 ± 0.03 MPa, $n = 8$ each, $P = 0.0347$, paired t test) and but had minimal effect on the energy loss ($51 \pm 3\%$ versus $57 \pm 8\%$, $n = 8$ each, $P = 0.2032$) (Fig. 6). Different stiffness in each principal direction can therefore be obtained when fibres are embedded in the rubber-like material.

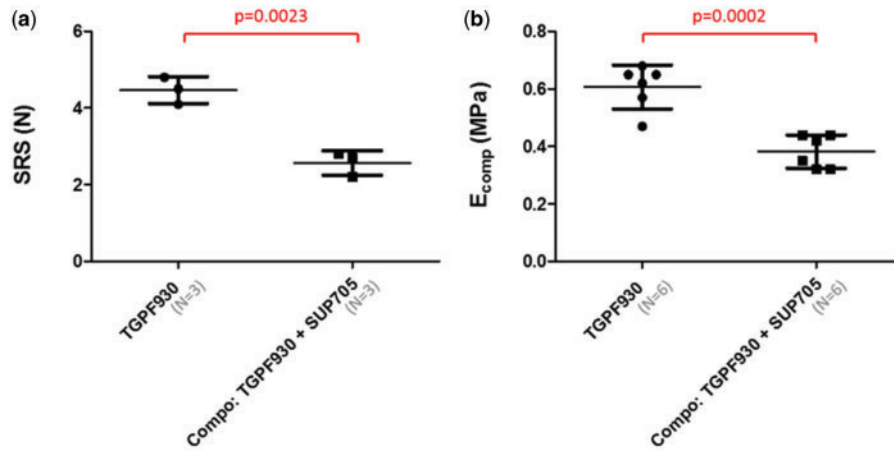


Fig. 4. (a) Suture retention strength (SRS) and (b) compressive modulus (E_{comp}) of pure Tangoplus FullCure 930 (TGPF930) and two-material composite (Tangoplus FullCure 930 [TGPF930] and support material [SUP705]). *P* values of unpaired t tests.

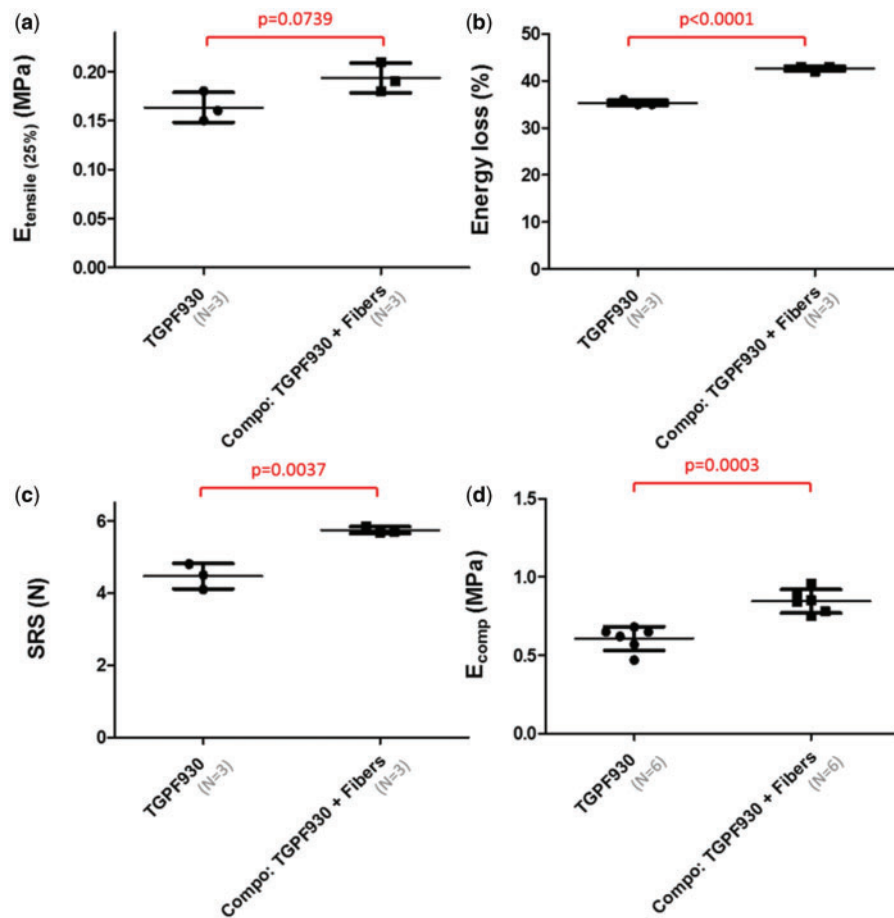
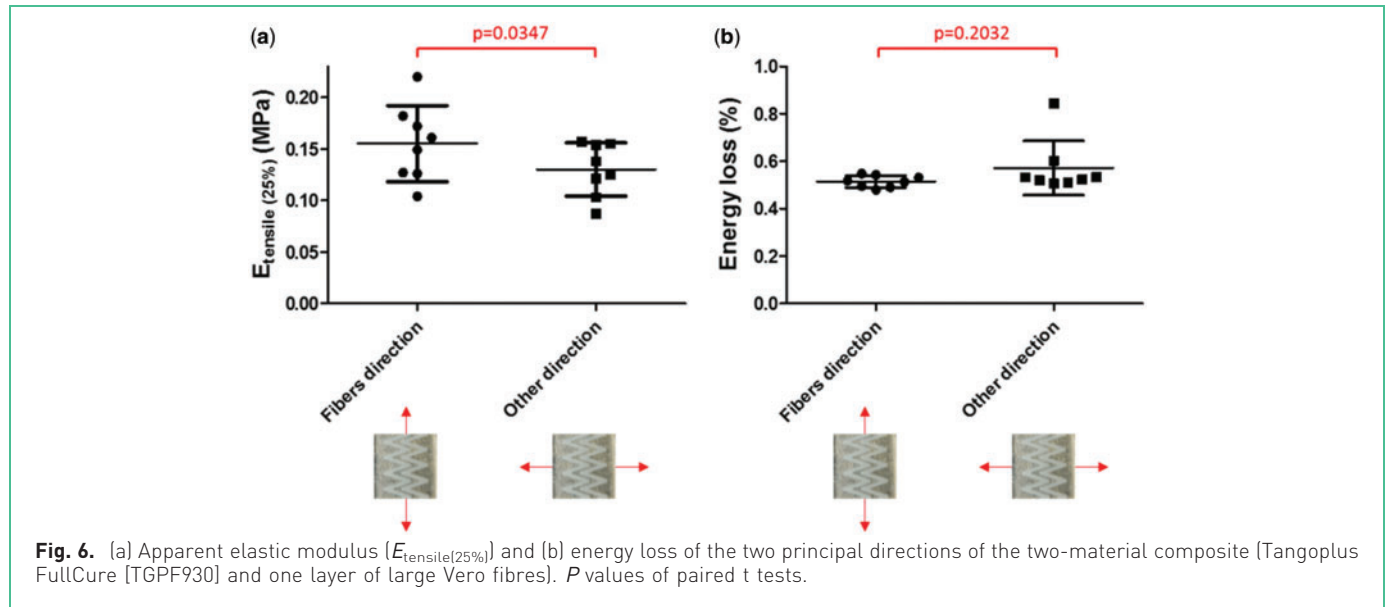


Fig. 5. (a) Apparent elastic modulus ($E_{tensile(25\%)}$), (b) energy loss, (c) suture retention strength (SRS) and (d) compressive modulus (E_{comp}) of pure Tangoplus FullCure 930 (TGPF930) and two-material composite (Tangoplus FullCure 930 [TGPF930] and two layers of rigid Vero fibres). *P* values of unpaired t tests.



Tunable, soft but strong three-material composite

Comparison with the 3D printed material

The above results were used to tune a three-material composite to create a synthetic aortic tissue. The results of a TGPF930 with two fibre layers (Vero White) material softened by support material (SUP705) are presented. There was no significant difference in the three-material composite with pure TGPF930 (unpaired t test) in terms of apparent elastic modulus (0.16 ± 0.02 MPa, $n = 5$, $P = 0.6010$) and SRS (4.25 ± 0.67 N, $n = 3$, $P = 0.6507$) (Fig. 7a–d). However, the energy loss ($40 \pm 3\%$, $n = 5$, $P = 0.0158$) was significantly higher and the compressive modulus (0.39 ± 0.03 MPa, $n = 6$, $P < 0.0001$) was lower. Consequently, adding support material (SUP705) softened the overall structure and increased the viscoelasticity. The fibres allow the material to maintain integrity and allow for tuning of the material anisotropy.

Comparison with the aortic tissue

The SRS (4.25 ± 0.67 N, $n = 3$, $P = 0.6177$) and compressive modulus (0.39 ± 0.03 MPa, $n = 6$, $P = 0.4485$ and $P = 0.0596$ for normal and aneurysmal aortas, respectively) of the three-material composite have shown similarities with the aortic tissue. The 25% strain apparent elastic modulus (0.16 ± 0.02 MPa, $n = 5$, $P = 0.0002$ and $P < 0.0001$ for normal and aneurysmal aortas, respectively) and energy loss ($39.92 \pm 2.27\%$, $n = 6$, $P < 0.0001$) (unpaired t test) were still significantly stiffer and more viscous than human AA (Fig. 7e–h).

When looking at the average loading curve of the three-material composite ($n = 6$) in comparison with normal

($n = 3$) and aneurysmal ($n = 4$) aortic tissues in tensile testing at lower strains, the properties are very similar (Fig. 8). By 25%, strain hardening of the composite occurs at a higher rate than in human tissue.

Discussion

The 3D printed material TGPF930 has been used in surgical education and is suitable in some applications. However, the material properties of TGPF930 are uniform and isotropic. To resolve this issue, we created 3D printable composites using TGPF930 to create synthetic AA tissue for surgical simulation. Mechanical testing was used to evaluate the tissue fidelity of our 3D printed models. The apparent elastic modulus and energy loss provide a measure of the dynamic response of the model due to the forces created by blood flow. The compressive modulus characterizes the feel or haptics, and the suture retention strength simulates the material's capacity to be sewn.

The study has shown how we can control the softness, strength, and mechanical directional dependency of the materials with a fibrous structure and the insertion of support material. However, there are limits to the mechanical properties that can be tuned with the currently available commercial materials. In the future, further fine-tuning can be done by varying the fibre geometries as well as the amount of filling in the soft structure. Despite the limitations, the mechanical properties of aortic tissue, such as the compressive stiffness and strength, were replicated with the three-material composite.

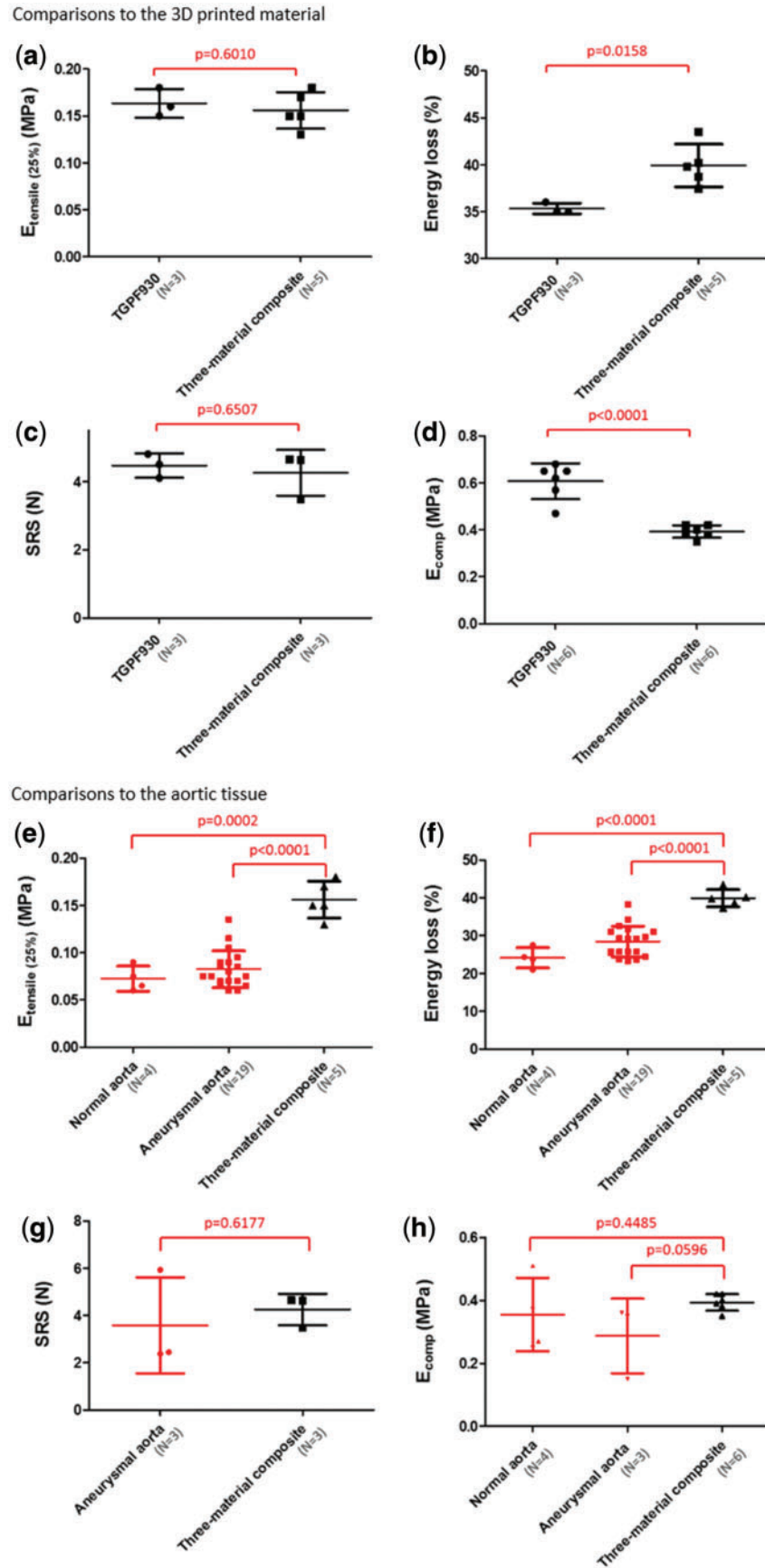


Fig. 7. Comparisons of the three-material composite with the 3D printed composite (a-d) and aortic tissue (e-h) in terms of apparent elastic modulus ($E_{\text{tensile}(25\%)}$) (a, e), energy loss (b, f), suture retention strength (SRS) (c, g), and compressive modulus (E_{comp}) (d, h). P values of unpaired t tests.

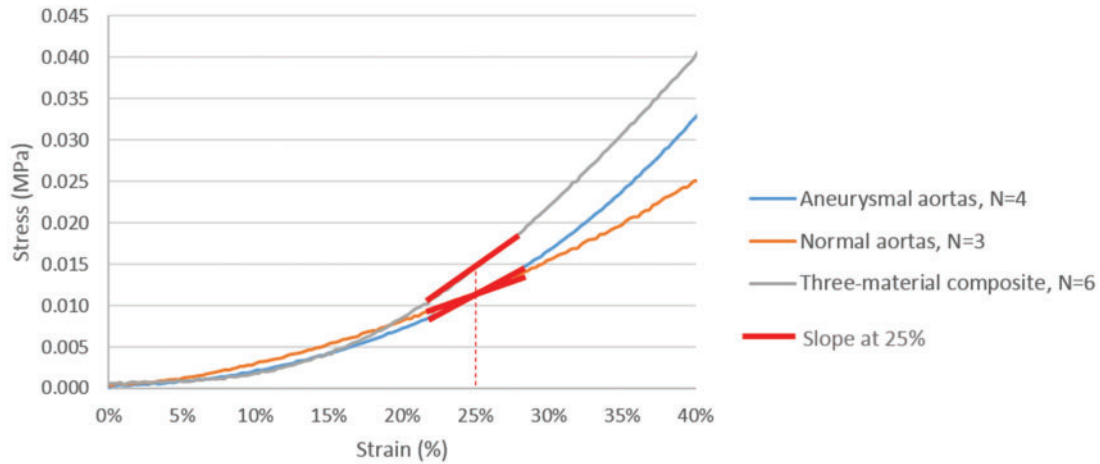


Fig. 8. Stress and strain loading curves of normal and aneurysmal aortas, as well as three-material composite.

We found the tensile properties of TGPF930 stiffer and more viscous than AA tissue but this may not be a fair comparison. The use of the same strain range for tensile testing assumes the samples start at a zero stress state. When AA tissue is excised, it demonstrates significant residual stress and recoils when cut. It is known that the physiologic strain of the aorta during a cardiac cycle is in the range of 5-10% due to blood pressure.^{13,14} To account for the residual stress in vivo, ex vivo biomechanical studies generally use higher strains (25%, 40% or maximum apparent elastic modulus) to identify the stiffness of the tissue.⁹ The 3D printed materials do not demonstrate significant residual stress when printed and we would likely only see such high strains due to surgical manipulation. Moreover, small differences in stiffness and energy loss may not be perceptible for surgical training. Future studies should examine the physiologic fidelity of the composites implemented in phantoms using pressure dilation testing, echocardiography imaging,¹⁵ strain imaging¹⁶ and subjective analysis of surgeons in training scenarios. In our study, we were able to reproduce the compressive modulus and SRS of ex vivo passive normal and aneurysmal AA tissue (Fig. 7e-h). Matching these properties will help ensure that the feel of manipulation and suturing are recreated in our synthetic models.

The novelty of our method is the ability to create heterogeneous and tunable composites using a commercial 3D Polyjet printer and materials. Despite the advancements in printing technology, commercial 3D printers do not allow the user to alter the polymer formulation, thus limiting the starting point for surgical simulation. Making combinations of materials is an alternative to controlling the polymer blend properties. To the best of our knowledge, this is the first study that has used support material to soften the structure.

Our analyses showed that the mechanical behaviour of the 3D printable composite is largely dominated by the properties of TGPF930 (apparent elastic modulus and energy loss). The fibres allow for adjusting the directional properties of the material and the support material softens the composite and increases its viscosity. Using 3D Polyjet printing, we can manipulate these properties to adjust the local material properties necessary to recreate thoracic aortic pathologies.

Pathologic AA tissue is heterogeneous and can show a significant loss of anisotropy due to the degeneration and remodelling of the walls.^{2,3} Fibres of collagen of normal tissue are at a slight angle from the circumferential direction of the artery but tend towards the principal directions in distension state.¹⁷ Those property variations between the principal directions of the tissue can be replicated with the use of fibres mimicking fibrous proteins such as collagen with different angular orientations.^{18,19} Pathologic tissue remodelling is also known to alter the AA collagen and elastin structure, resulting in large variations in material properties among patients. This medical degeneration changes the anisotropy of the tissue.^{2,3} Therefore, adjusting these local properties could be key to tissue fidelity in aortopathies.

Others have used multi-material composites to alter the mechanical properties of 3D printed models made with Polyjet technology. A recent study developed 3D printed microcells made of hard elliptical or ellipsoid-like fibres (non-specified materials) randomly distributed in a soft TGPF930 matrix in order to improve micromechanical models used in finite element analyses for numerical simulations.²⁰ Materials were evaluated in tensile and compressive testing but were not compared with biological tissues. Similarly, Wang et al.²¹ combined soft (TGPF930) and rigid

Vero materials for soft patient-specific tissue-mimicking phantoms but neglected the mechanical directional dependency of the overall structure by using fibres in only one direction. They also limited the assessment of their 3D printing multi-materials to uniaxial testing only, which may not be enough for a proper validation and representation of potentially anisotropic biological tissues. In addition, Vukicevic et al.⁶ mixed both materials (TGPF930 and Vero) during the printing in order to change the hardness of the model. Two blends were created to differentiate the external structure and inner core of the valve leaflets in a model used for mitral valve repair strategies. However, both resulting materials remained homogeneous and isotropic, which could potentially be a major limitation for a proper representation of soft tissue, as mentioned above.

We have implemented the three-material composite in a patient-specific aortic geometry obtained by imaging data with the method developed by Garcia et al.²² To further our development, the 3D patient-specific aortic models with high tissue fidelity need to be evaluated by experienced surgeons to validate the best combinations for task-specific vascular surgical training.

Beyond aortic surgery, the tunable 3D printed material could be used for other applications. Alterations of the composite structure would potentially allow accurate representations of other soft tissues and whole organs. These phantoms will also be very useful for evaluating medical devices and imaging techniques.

Conclusion

In this study, we reported that mechanical properties of 3D printed composites (e.g. hardness, apparent elastic modulus, energy loss, compressive modulus and SRS) can be controlled and adjusted by using rigid fibres and brittle support material. We replicated the ex vivo passive tissue characteristics of aortas, and therefore were able to improve the current homogeneous 3D printed TGPF930 material often used in surgical education.

Conflict of interest

None declared.

Acknowledgements

We gratefully thank the Research Institute of the McGill University Health Centre (MUHC) for their assistance in this project and McGill University for the financial support.

References

1. Malik HH, Darwood ARJ, Shaunak S, Kulatilake P, El-Hilly AA, Mulki O, et al. Three-dimensional printing in surgery: a review of current surgical applications. *J Surg Res* 2015; 199: 512–522. <https://doi.org/10.1016/j.jss.2015.06.051>.
2. Chung J, Lachapelle K, Cartier R, Mongrain R, Leask RL. Loss of mechanical directional dependency of the ascending aorta with severe medial degeneration. *Cardiovas Pathol* 2017; 26: 45–50. <https://doi.org/10.1016/j.carpath.2016.11.001>.
3. Shahmansouri N, Alreshidan M, Emmott A, Lachapelle K, El-Hamamsy I, Cartier R, et al. Investigation on the regional loss factor and its anisotropy for aortic aneurysms. *Materials* 2016; 9: 867. <https://doi.org/10.3390/ma9110867>.
4. Kurenov SN, Ionita C, Sammons D, Demmy TL. Three-dimensional printing to facilitate anatomic study, device development, simulation, and planning in thoracic surgery. *J Thorac Cardiovasc Surg* 2015; 149: 973–979. <https://doi.org/10.1016/j.jtcvs.2014.12.059>.
5. Biglino G, Verschuere P, Zegels R, Taylor AM, Schievano S. Rapid prototyping compliant arterial phantoms for in-vitro studies and device testing. *J Cardiovasc Magn Reson* 2013; 15: 2–7. <https://doi.org/10.1186/1532-429X-15-2>.
6. Vukicevic M, Puperi DS, Grande-Allen KJ, Little SH. 3D printed modeling of the mitral valve for catheter-based structural interventions. *Ann Biomed Eng* 2017; 45: 508–519. <https://doi.org/10.1007/s10439-016-1676-5>.
7. Wurm G, Lehner M, Tomancok B, Kleiser R, Nussbaumer K. Cerebrovascular biomodeling for aneurysm surgery: simulation-based training by means of rapid prototyping technologies. *Surg Innov* 2011; 18: 294–306. <https://doi.org/10.1177/1553350610395031>.
8. Yang Z. Development of 3D printed patient specific ascending aortic training models for cardiac surgery. Doctoral dissertation, McGill University Libraries; 2016.
9. Emmott A, Garcia J, Chung J, Lachapelle K, El-Hamamsy I, Mongrain R, et al. Biomechanics of the ascending thoracic aorta: a clinical perspective on engineering data. *Can J Cardiol* 2016; 32: 35–47. <https://doi.org/10.1016/j.cjca.2015.10.015>.
10. Pazos V, Mongrain R, Tardif JC. Polyvinyl alcohol cryogel: optimizing the parameters of cryogenic treatment using hyperelastic models. *J Mech Behav Biomed Mater* 2009; 2: 542–549. <https://doi.org/10.1016/j.jmbbm.2009.01.003>.
11. Chung J, Lachapelle K, Wener E, Cartier R, De Varennes B, Fraser R, et al. Energy loss, a novel biomechanical parameter, correlates with aortic aneurysm size and histopathologic findings. *J Thorac Cardiovasc Surg* 2014; 148: 1082–1089. <https://doi.org/10.1016/j.jtcvs.2014.06.021>.
12. Oliver WC, Pharr GM. An improved technique for determining hardness and elastic modulus using load and displacement sensing indentation experiments. *J Mater Res* 1992; 7: 1564–1583. <https://doi.org/10.1557/JMR.1992.1564>.

13. Morrison TM, Choi G, Zarins CK, Taylor CA. Circumferential and longitudinal cyclic strain of the human thoracic aorta: age-related changes. *J Vasc Surg* 2009; 49: 1029–1036. <https://doi.org/10.1016/j.jvs.2008.11.056>.
14. Grøndal N, Bramsen MB, Thomsen MD, Rasmussen CB, Lindholt JS. The cardiac cycle is a major contributor to variability in size measurements of abdominal aortic aneurysms by ultrasound. *Eur J Vasc Endovasc Surg* 2012; 43: 30–33. <https://doi.org/10.1016/j.ejvs.2011.09.025>.
15. Maragiannis D, Jackson MS, Igo SR, Schutt RC, Connell P, Grande-Allen J, et al. Replicating patient-specific severe aortic valve stenosis with functional 3D modeling. *Circ Cardiovasc Imaging* 2015; 8: e003626. <https://doi.org/10.1161/CIRCIMAGING.115.003626>.
16. Petrini J, Eriksson MJ, Caidahl K, Larsson M. Circumferential strain by velocity vector imaging and speckle-tracking echocardiography: validation against sonomicrometry in an aortic phantom. *Clin Physiol Funct Imaging* 2018; 38: 269–277. <https://doi.org/10.1111/cpf.12410>.
17. Gasser TC, Ogden RW, Holzapfel GA. Hyperelastic modeling of arterial layers with distributed collagen fibre orientations. *J R Soc Interface* 2006; 3: 15–35. <https://doi.org/10.1098/rsif.2005.0073>.
18. Chen H, Liu Y, Slipchenko MN, Zhao X, Cheng J-X, Kassab GS. The layered structure of coronary adventitia under mechanical load. *Biophys J* 2011; 101: 2555–2562. <https://doi.org/10.1016/j.bpj.2011.10.043>.
19. Finlay HM, McCullough L, Canham PB. Three-dimensional collagen organization of human brain arteries at different transmural pressures. *J Vasc Res* 1995; 32: 301–312. <https://doi.org/10.1159/000159104>.
20. Reiter M, Major Z. A combined experimental and simulation approach for modelling the mechanical behaviour of heterogeneous materials using rapid prototyped microcells. *Virtual Phys Prototyp* 2011; 6: 111–120. <https://doi.org/10.1080/17452759.2011.586949>.
21. Wang K, Wu C, Qian Z, Zhang C, Wang B, Vannan MA. Dual-material 3D printed metamaterials with tunable mechanical properties for patient-specific tissue-mimicking phantoms. *Addit Manuf* 2016; 12(Part A): 31–37. <https://doi.org/10.1016/j.addma.2016.06.006>.
22. Garcia J, Yang ZL, Mongrain R, Leask RL, Lachapelle K. 3D printing materials and their use in medical education: a review of current technology and trends for the future. *BMJ Simul Technol Enhanc Learn* 2017; 4: 27–40. <https://doi.org/10.1136/bmjstel-2017-000234>.